buildings

MDPI

Article

Assessing the Impact of Ground Motion Duration on Losses in Typical Modern Steel Moment Frames

Amir Safiey [1,*], Sereen Majdalaweyh [2] and Weichiang Pang [3]

[1] CoreLogic, 40 Pacifica, Irvine, CA 92618, USA
[2] Karen Clark and Company, Boston, MA 02116, USA; smajdal@g.clemson.edu
[3] Glenn Department of Civil Engineering, Clemson University, Clemson, SC 29634, USA; wpang@clemson.edu
* Correspondence: amir.safiey@gmail.com

Abstract: This research was undertaken to study the duration effects on the seismic economic risk of steel moment frame (SMF) buildings, a prominent class of buildings in commercial stock. Firstly, a modified version of FEMA P-695 ground motion scaling, tailored for seismic loss estimation purposes and incorporating two sets of spectrally matched bi-directional short- and long-duration ground motions, is proposed to study code-compliant plan-symmetrical SMFs with different heights (i.e., two to 20 stories). It is shown that long-duration ground motions increase the collapse risk of SMFs, on average, by 28.0% at the MCE level. Next, a component-based loss estimation methodology was adopted for evaluating the seismic losses under each set of ground motions. These losses are studied separately for building components (i.e., structural and nonstructural) and contents. Moreover, we propose an approach for calculating average annualized loss (AAL) as a prominent risk meter that segregates contributions of short- and long-duration ground motions to attain hazard consistency. Loss analyses showed the minimal impact of building height on the contribution of these two types of earthquakes. The seismic risk analysis of buildings also revealed that collapse risk is influenced mainly by duration effects followed by building and content losses.

Keywords: performance-based earthquake engineering; insurance risk analysis; long-duration earthquake; subduction zones; seismic loss analysis

check for updates

Citation: Safiey, A.; Majdalaweyh, S.; Pang, W. Assessing the Impact of Ground Motion Duration on Losses in Typical Modern Steel Moment Frames. *Buildings* **2024**, *14*, 1373. https://doi.org/10.3390/buildings14051373

Academic Editors: Nicola Impollonia, Francesco Cannizzaro, Teresa Lombardo and Alessandro Palmeri

Received: 17 March 2024
Revised: 1 May 2024
Accepted: 2 May 2024
Published: 11 May 2024

1. Introduction

Duration is a key characteristic of ground motions. The strong shaking during a moderate or large earthquake typically lasts 10 to 30 s; however, at certain seismic zones (e.g., subduction), faulting systems can trigger strong ground motions that typically have a much longer duration, e.g., greater than 1 min. Modern buildings are designed in accordance with seismic codes and regulations that generally do not take long-duration earthquakes into consideration [1]. Extensive destruction to buildings and infrastructures brought about by long-duration seismic events, like those occurring in Maule, Chile, in 2010 and Tohoku, Japan, in 2011, has raised considerable concerns among researchers, insurance carriers, business owners, authorities, and property managers. A quick look at a world map showing major subduction faults reveals that large cities and associated critical infrastructures, including important metropolitan areas on the west coast of the United States (e.g., Seattle, WA, USA), are highly exposed to long-duration severe ground shaking. Loss assessment methodologies, however, such as FEMA's HAZUS-MH methodology [2], do not explicitly consider the ground-motion duration effects on seismic losses.

Over the past decades, various researchers have studied the effects of ground motion duration on the seismic performance of buildings. An early study conducted by van de Lindt and Goh revealed the significant impact of long-duration ground motions on the reliability of structural systems [3]. More recently, researchers have employed incremental dynamic analysis (IDA) more extensively to study the impact of ground motion duration

on the seismic performance of structural systems. However, to quantify the impact of long-duration compared with short-duration shakings, the spectral shape effect needs to be isolated by considering two separate representative ensembles of spectrally matched ground motions. In this way, insights can be obtained into the relative impact of ground motion duration. Many researchers have utilized this approach to gauge duration effects using single degree of freedom (SDOF) modeling [4–7] on the seismic performance of different structural systems, including bridges [8], reinforced concrete structures [9–11], and light-frame wood constructions [12–15]. In terms of steel moment frames, the focus of the current study, Liapopoulou et al. [7], Chandramohan et al. [16], and Hwang et al. [17] found that long-duration ground motions resulted in a relatively 20%, 29%, and 43% reduction in median collapse capacity (i.e., median spectral acceleration of collapse at the fundamental period of buildings), respectively. Additionally, Zengin et al. [18] reported that long-duration earthquakes amplify the mean annual frequency of collapse of SMFs by 3.5 times when compared to corresponding short-duration earthquakes. Overall, these studies prove the detrimental impact of long-duration earthquakes on structural systems in terms of collapse fragility and damage index.

As briefly mentioned above, a comprehensive literature review showed that most studies conducted on duration effects stopped short of studying seismic losses, particularly nonstructural and content damage and loss. Understanding how duration affects seismic losses could be of great significance in assessing seismic risk and the resilience of communities. Hence, this study proposes an overall seismic performance-based assessment framework that considers spectrally matched long-duration earthquakes.

More recently, Hwang et al. [17] studied the effects of long-duration earthquakes on the seismic collapse risk and losses of four modern steel structures utilizing the ground motions from work by Chandramohan et al. [16]. The current authors' similar study on light-frame wood buildings revealed the considerable impact ground motions had on incurred losses [19]. It is worth mentioning that these studies incorporate two sets of ground motions in which horizontal components of different ground motions are mixed and matched. Even though such ground motion ensembles are utilized for loss estimation [17], this practice does not seem sound because seismic loss estimation requires predicting seismic responses in the two main orthogonal directions. Belejo et al. extended Chandramohan et al.'s approach for 3D structural analyses by spectrally matching the geomean of two orthogonal rotated short-duration components with the as-recorded long-duration components [20]. Although this strategy seems promising, it may not be effective for all ground motions, especially unpolarized ones, as defined by Shahi and Baker [21]. As a result, this study proposes a modified version of the well-known FEMA P-695 scaling procedure that incorporates a spectral matching approach by matching the geometric means of both horizontal components of short-duration and long-duration pairs [21]. Furthermore, Otarola et al. investigated the influence of ground motion duration on seismic losses in SDOFs and RC frames through a simplified approach utilizing damage-to-loss ratios and system-level fragility functions—similar to the HAZUS-MH approach. However, they did not differentiate between losses attributed to structural, non-structural, and content elements [22,23].

To address the issue under research, an understanding is needed of the effects of subduction earthquakes on steel structures of different heights as well as the loss associated with two primary insurance coverages (i.e., building and content) of a building property. The current study was undertaken on modern commercial buildings with steel moment frames, one of the leading commercial construction types. As high-rise buildings are unlikely to collapse, how building height affects financial losses from events other than collapse is a critical issue [24]. At the outset, this paper proposes a modified version of the FEMA P-695 [25] ground motion scaling procedure to pave the way for studying the influence of ground motion duration on the expected loss. First, a bi-directional, spectrally matched database of 50 ground motions corresponding to 25 long- and 25 short-duration ground motions is designated. Thereafter, the modified approach is employed to conduct

IDA on steel moment frame archetypes with heights ranging from two to 20 stories designed for a high seismic region. Next, the structural analysis results are relayed to a building-specific loss assessment framework developed based on FEMA P-58 provisions [26] to assess the impact of different ground motion durations on structural and nonstructural components as well as content losses, separately. Average annual loss (AAL) is a vital risk index applied to quantify losses and make financial-related decisions (e.g., determining insurance rates). This paper proposes an effective approach to computing AAL, which segregates the contribution of short- and long-duration earthquakes and helps derive a hazard-consistent estimate of AAL, as urged in an earlier study [17].

2. Selecting and Scaling Ground Motions

Selecting and scaling ground motions are crucial for predicting a building's seismic response to quantify its seismic performance. FEMA P-695 provisions are widely used in IDA, which recommends a selecting and scaling method consisting of two main steps, i.e., normalizing and group scaling. The P-695 approach, however, does not account for long-duration (i.e., subduction zone) ground motions. Moreover, the spectral matching technique is used to study duration effects [16], whereby each horizontal component of long-duration ground motions is matched with a horizontal component of short-duration ground motions based on spectral shape. This study proposes a modified version of FEMA P-695 suitable for spectral matching technique and seismic loss analysis.

2.1. Selection of Ground Motions

Twenty-five bi-directional ground motion records were collected from the PEER NGA-West2 [27], K-Net, and Kik-net databases [28], and the Consortium of Organizations for Strong-Motion Observation Systems (COSMOS) Virtual Data Center [29]. Subduction earthquakes included long-duration earthquakes from nine events. The records are characterized by significant durations of 5% to 95% ($D_{5–95\%}$); this parameter is defined as the time interval between accumulated Arias intensity (I_a) of 5.0% and 95.0%, as described elsewhere [16], as shown in Figure 1.

Records with a significant duration of $D_{5–95\%}$ longer than 30 s were classified as long-duration [16]. The proposed methodology for the selection of the short-duration records comprises the following steps:

Step 1: Select a source (e.g., PEER NGA-West2 database) for short-duration ground motions. The short-duration records are classified as those with a significant duration ($D_{5–95\%}$) of less than 30 s.

Step 2: Compute 5% damped elastic response spectra for each pair of as-recorded short-duration and as-recorded long-duration records. Then, find the geometric mean of the orthogonal response spectra for both long- and short-duration pairs. Finally, select a matching factor (*MF*) that yields the minimum sum of the squared error (*SSE*) as follows:

$$SSE = \sum_{i=1}^{N} \left((MF) Sa_{gm}^{LD}(T_i) - Sa_{gm}^{SD}(T_i) \right) \tag{1}$$

where $Sa_{gm}^{LD}(T_i)$ is the geomean spectral acceleration ordinate at each discretized period T_i corresponding to as-recorded long-duration components, $Sa_{gm}^{SD}(T_i)$ is the geomean spectral acceleration ordinate at each discretized period T_i corresponding to the as-recorded short-duration records, and N is the number of the period intervals. The period range of interest is $0.05 < T < 5.0$ s to include low-, mid-, and high-rise structures.

Step 3: For the short-duration set, normalize the short-duration pairs according to the FEMA P-695 procedure. For each short-duration record (j), find the peak ground velocity (PGV_j) for both orthogonal components. Then, determine the geometric mean of both components ($PGV_{gm,j}$). The normalization factor (NM_j) is:

$$NM_j = \frac{\widehat{PGV_{gm}}}{PGV_{gm,j}} \tag{2}$$

where $\widehat{PGV_{gm}}$ is the median of $PGV_{gm,j}$ values for the set of ground motions. Normalization reduces record-to-record variability, which alleviates the need for a large number of ground motion records. Both short-duration orthogonal components are multiplied by the same normalization factor to preserve the relative strength of each ground motion component [25]. Figure 2 presents the natural log of response spectra of 50 individual short-duration records (25 pairs), the natural log median, and two natural log standard deviations (LnSTRDev).

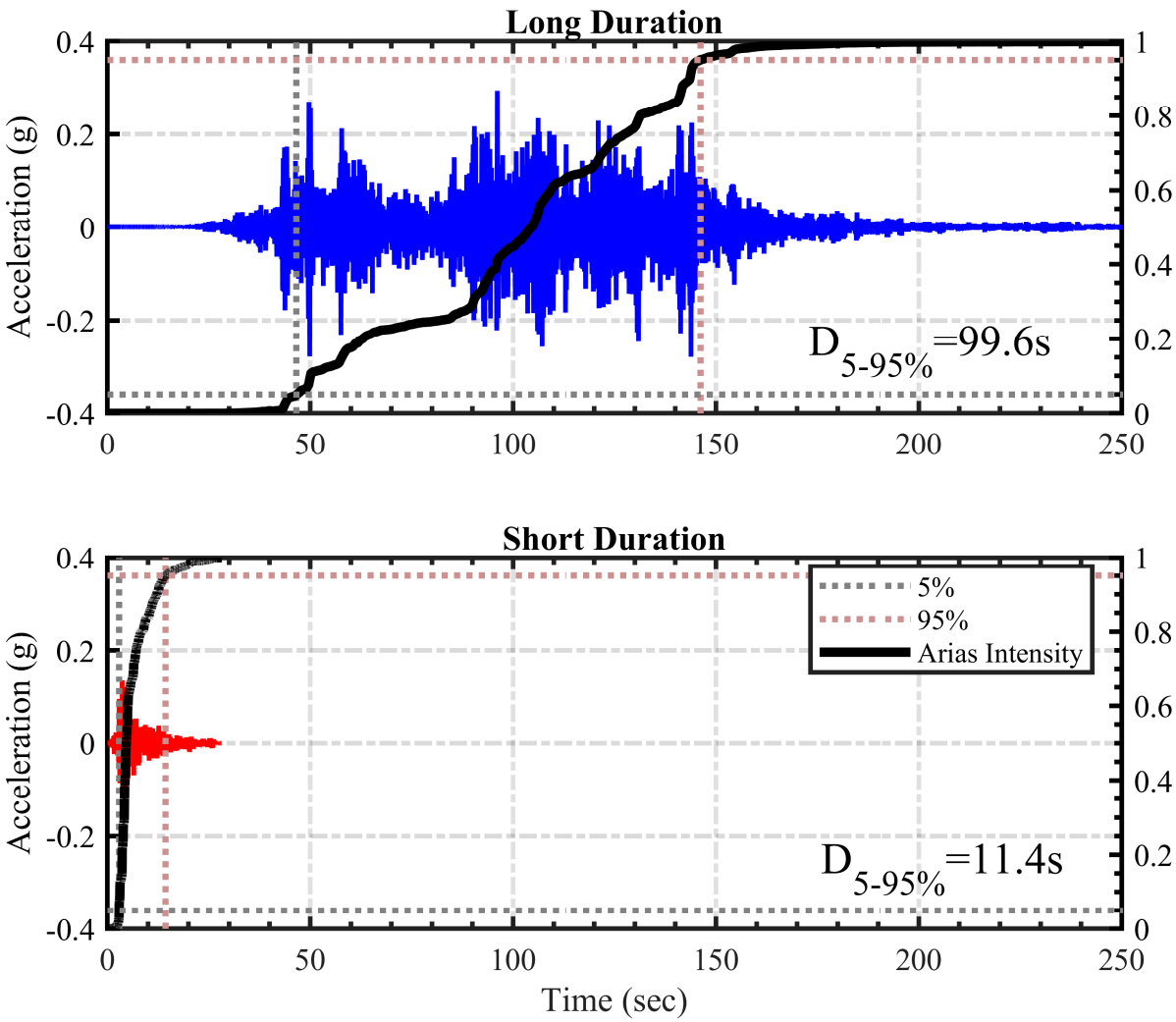

Figure 1. Arias intensity and significant duration $D_{5–95\%}$ of long- and short-duration ground motions of the third pair of ground motions listed in Appendix A.

Step 4: Repeat Step 2, but this time for each pair of the normalized short-duration and as-recorded long-duration records, compute the elastic response spectra at 5% damping, then find the geometric mean of the orthogonal response spectra for both long- and short-duration pairs. Finally, select the new matching factor (*MF*) that yields the minimum *SSE*. Figure 3 displays the matched geometric response spectra of the third pair of long- and short-duration ground motions and those corresponding to components.

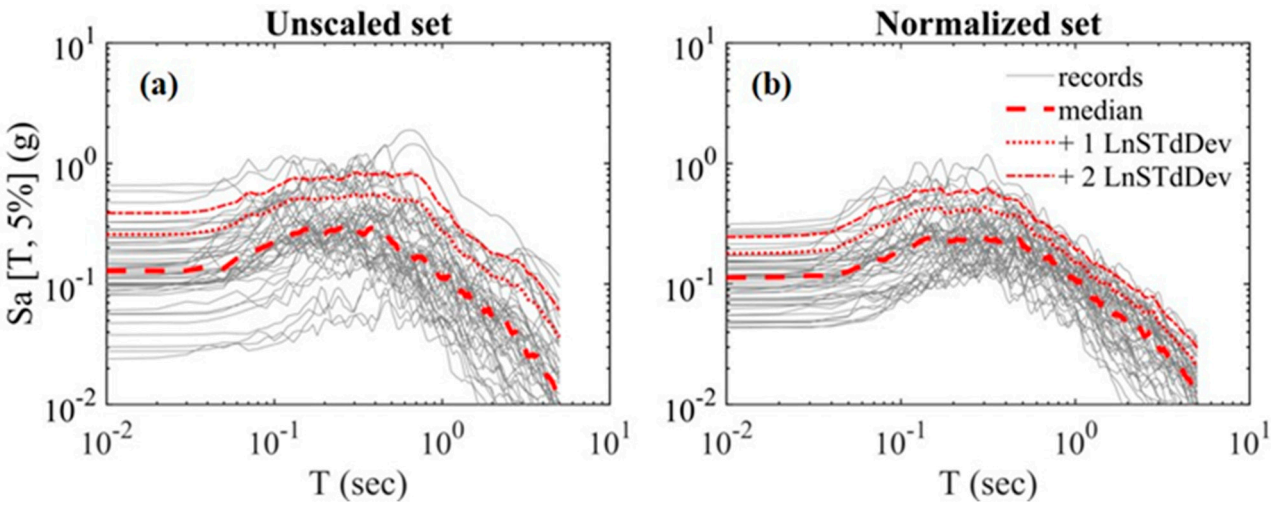

Figure 2. Response spectra of 50 individual short-duration records, median, and one and two standard deviations of the total set: (**a**) response spectra of unscaled (raw) short-duration set; (**b**) response spectra of normalized short-duration set. LnSTdDev is the natural log standard deviation. Sa is spectral acceleration.

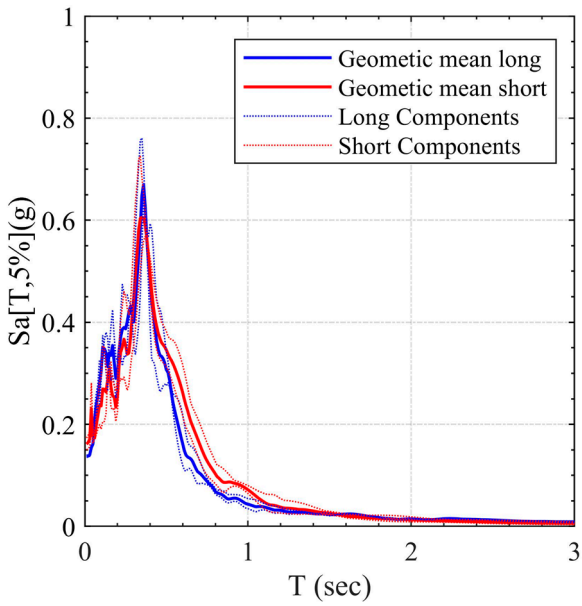

Figure 3. Matched response spectra for the 3rd earthquake pair, including the individual components and the geometric means of long and short durations.

Appendix A lists the selected pairs of long-duration and short-duration earthquake records as well as normalization and matching factors. In this work, we adopted predefined matched pairs of long and short records handpicked from the previous literature. It is worth mentioning that pulse-like ground motions are eliminated. Figure 4 presents an overview of various key characteristics of selected short- and long-duration ground motions in terms of $D_{5\text{–}95\%}$, magnitude (M_w), and rapture distance (R_{rup}). Figure 5 shows the median of the geometric mean of long- and short-duration spectra, revealing a good match between them.

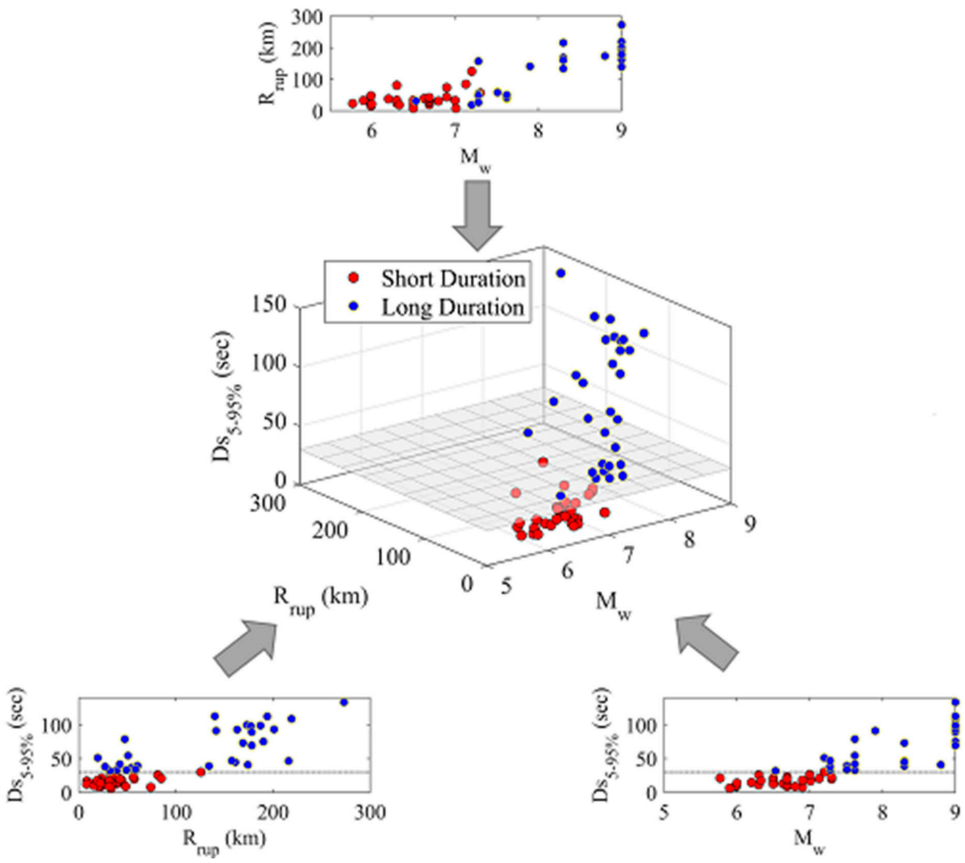

Figure 4. An overview of important characteristics of the selected short- and long-duration ground motions, i.e., $D_{s5–95\%}$, magnitude (M_w), and rapture distance (R_{rup}), incorporating the boundary between short- and long-duration ground motions. $D_{s5–95\%}$ is significant durations of 5% to 95%. The grey line and grey plane represent the border between short-duration and long-duration ground motions.

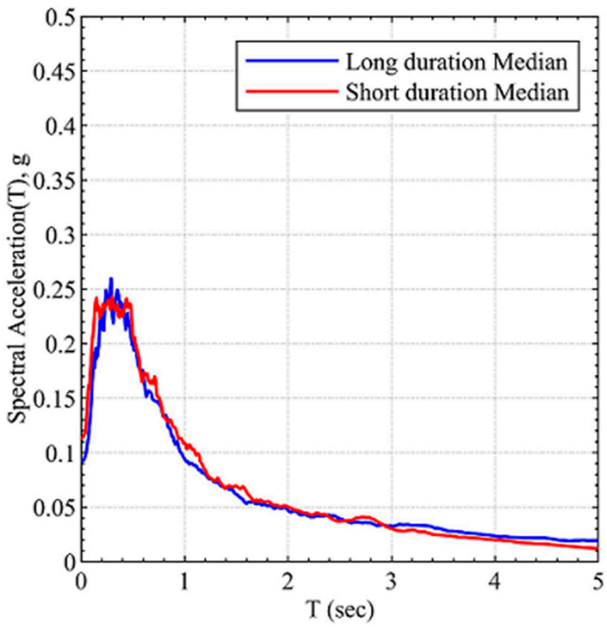

Figure 5. Median response spectra for the geometric mean of long- and short-duration ground motions.

2.2. Group Scaling

FEMA P-695 scaling procedure requires the spectrum of normalized selected ground motions to be scaled altogether to a series of select incrementally increasing spectral accelerations using group factor (*GF*) to conduct the IDA and evaluate the collapse capacity of the building. In a nutshell, the final scaling factor (*SF*) can be calculated from:

$$STH^{LD} = SF_{LD} \cdot TH^{LD} = MF \cdot GF \cdot TH^{LD} \quad (3)$$

$$STH^{SD} = SF_{SD} \cdot TH^{SD} = NM \cdot GF \cdot TH^{SD} \quad (4)$$

where SF_{SD} and SF_{LD} are defined as the final short-duration and long-duration scaling factors, respectively; TH^{SD} and TH^{LD} are the time history of each component and each short- and long-duration ground motion, respectively; and *GF* is the group factor. STH^{SD} and STH^{LD} are the scaled time history of each component and each short- and long-duration ground motion, respectively. More details can be found in FEMA P-695.

3. Studied Steel Moment Frame Buildings

The west coast of the United States is prone to long-duration ground shakings because of the proximity of subduction fault systems in the Pacific Ocean. Important cities in the region, like Seattle, WA, are centers of many vital industries. Steel construction in this area is known to play a dominant role in commercial building stock [30]. Studies have also shown that ductile buildings are more drastically influenced by long-duration ground motions than non-ductile buildings [11]. The current study is devoted to modern steel moment frames designed for high seismic regions, or seismic design category (SDC) D [31], and assumes that such buildings are located in Seattle, WA. Modeling is conducted using the OpenSees software package [32]. The lateral system of the buildings is a perimeter moment frame with reduced beam section (RBS) connections, which are widely used prequalified steel moment connections [33].

To investigate the effects of building height, five buildings with 2, 4, 8, 12, and 20 stories were selected and referred to as SMF2, SMF4, SMF8, SMF12, and SMF20, respectively. The building footprint was 42.7 m by 30.5 m; the typical story height was 4 m, but the first story was 4.6 m high. Figure 6 presents the layout and elevation view of the building archetype. The five buildings were simulated with a phenomenological modeling approach incorporating two sets of nonlinear springs, the first of which accounts for the flexural nonlinearities of steel members, including cyclic deterioration through the Ibarra–Medina–Krawinkler (IMK)'s modified deterioration model [34], and the second for the shear nonlinearity of the panel zone region through Gupta and Krawinkler's trilinear model [34]. The models consider the contributions of the gravity system and composite action. The models also take P-Delta effects into consideration by incorporating leaning columns. Further details about the models, including ductility, mode shapes, and plastic hinge formation, can be found elsewhere [35–37].

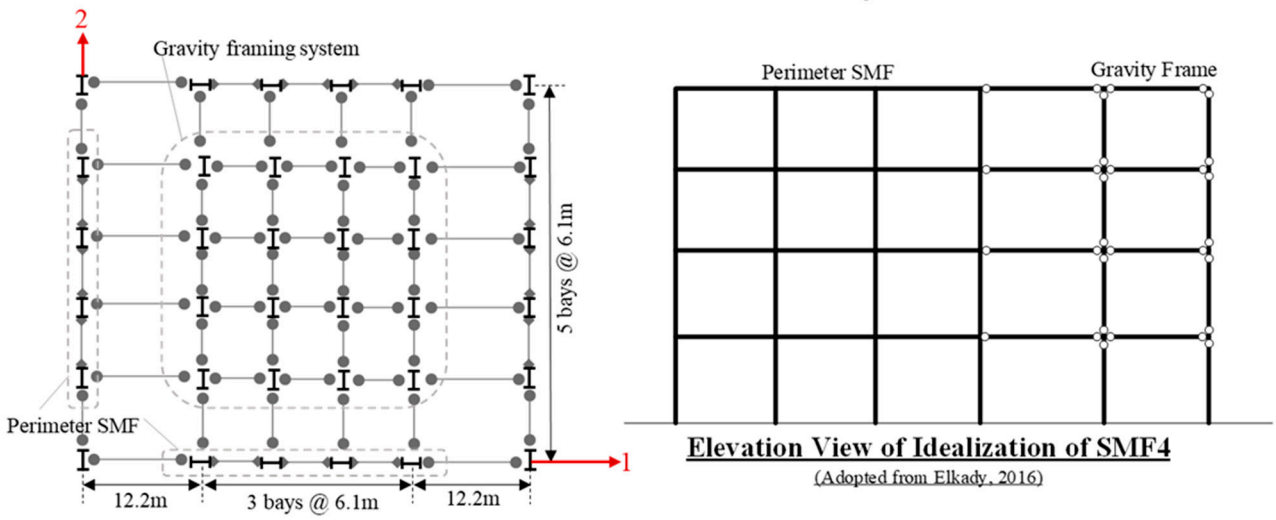

Figure 6. Layout including building dimensions and elevation view of the steel moment frame buildings [35].

The fundamental periods for the five models were determined to be 0.68 s, 1.31 s, 1.81 s, 2.45 s, and 3.18 s, respectively, using eigenvalue analysis. IDA was conducted for each building separately for the ensemble of short- and long-duration ground motions. Each ground motion was scaled up incrementally using 5% spectral damping acceleration at the fundamental period of the building until collapse was reached. We adopted the non-simulated collapse strategy, by which the collapse is defined as the maximum story drift ratio exceeding a certain limit (i.e., 10%) or the story shear resistance becoming zero. Figure 7 compares the dynamic capacity curves (i.e., IDA curves) for each building for short- and long-duration ground motions. The IDA curves represent the relationship between the maximum story drift ratio and the fundamental period's spectral acceleration. The collapse capacity of the buildings is characterized based on the IDA results in terms of median collapse spectral acceleration ($\hat{S_{CT}}$) and the associated dispersion. As can be seen, all buildings subjected to long-duration sets had a lower collapse capacity than those exposed to short-duration sets. On average, the median collapse spectral acceleration of a building is 28% lower under long-duration ground motions. Generally, SMF4 had a lower median collapse capacity than SMF2, because its overstrength is lower than that of SMF2 [35].

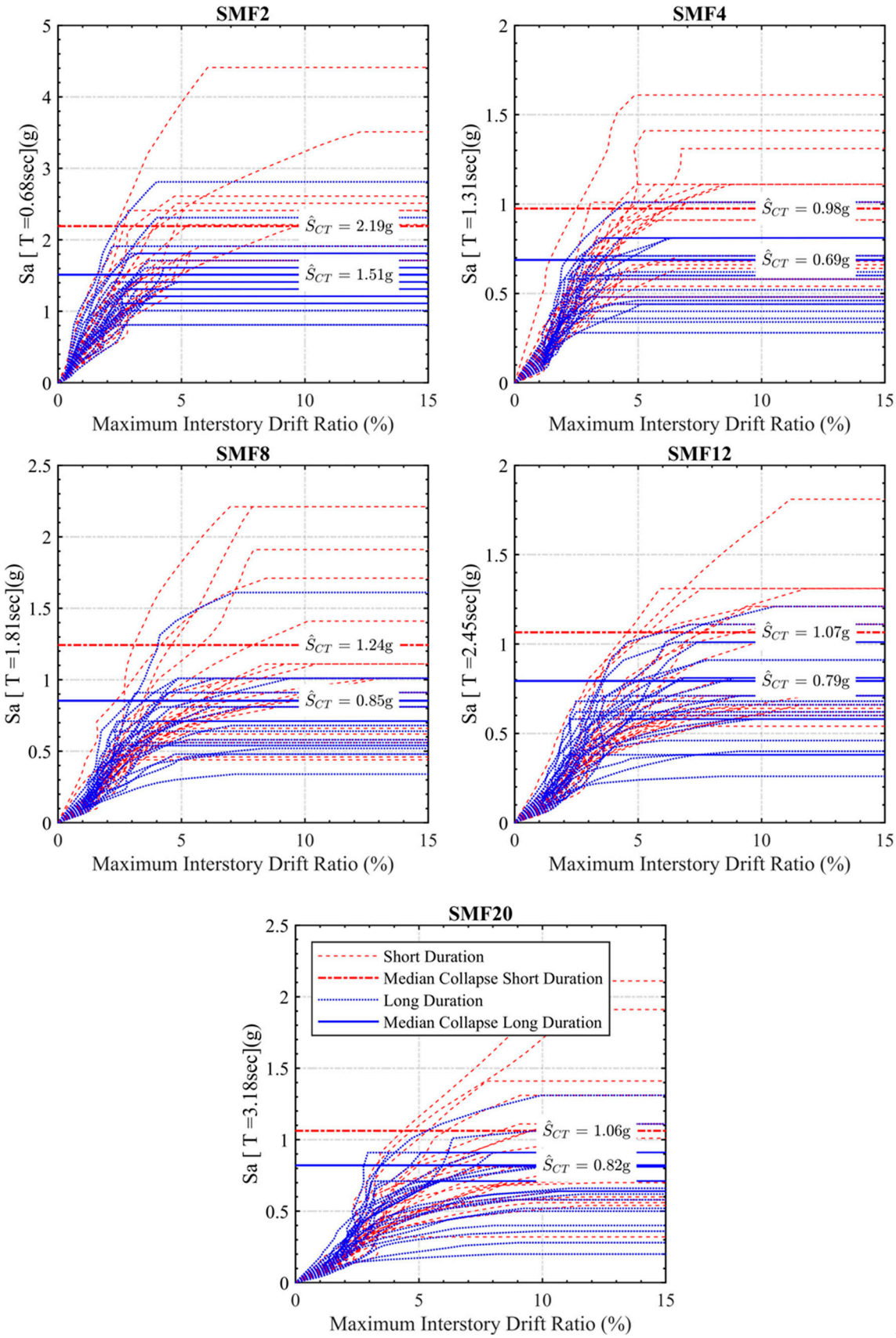

Figure 7. The IDA curves of the studied buildings subjected to long-duration and short-duration sets, separately presented for each building.

4. Loss Assessments

The seismic loss of the building archetypes was computed using a component-based loss assessment framework which utilizes the FEMA P-58 [26] methodology relying on the framework by the Pacific Earthquake Engineering Research (PEER) Center. The framework partitions the whole risk assessment domain into four subdomains, i.e., hazard, structural, damage, and loss analyses, interconnected in a Markov chain manner. The last two analyses, i.e., loss and damage, were merged and are referred to herein as the loss assessment framework. The framework consists of three separate sequential modules, namely the collapse check, irreparability check, and component-wise loss calculation. Loss assessment was performed using a previously developed MATLAB-based [38] computational platform called Apocalyptic Structural Assessment Program (ASAP) and implemented on the high-performance computing facilities of Clemson University, dubbed the Palmetto Cluster [39]. FEMA P-58 provides minimal content component fragility functions in its database. Therefore, content fragility and consequence functions were developed for this study based on earlier work [40] and added to the ASAP's clearinghouse. The toolbox was used extensively for loss estimation purposes, e.g., [41]. Losses made by the adopted archetypes' structural, nonstructural, and content components were studied; however, the losses sustained by the building (i.e., structural and nonstructural components) and its content were treated separately, according to the norm of insurance risk modeling.

Loss due to structural collapse is a main contributor to building and content losses. It is predicted by considering the collapse fragility of a structure idealized using the lognormal cumulative distribution function without any adjustment for spectral shape. FEMA P-58 provisions emphasize incorporation with three-dimensional modeling of structures. In this study, two-dimensional nonlinear modeling was adopted because the lateral force resisting system of each building consists of two uncoupled perimeter moment frames. The seismic responses of each building can be reasonably modeled using a separate two-dimensional moment frame in each of the lateral directions (Figure 6). The probability of building collapse at a given intensity measure, assuming the collapses of the two moment frames are statistically independent (S.I.), is computed as:

$$P_{2D}(C|IM) = \frac{n_{C1}}{n_{GM}} + \frac{n_{C2}}{n_{GM}} - \frac{n_{C1}}{n_{GM}}\frac{n_{C2}}{n_{GM}} \tag{5}$$

where $P_{2D}(C|IM)$ is the building collapse probability at a given intensity measure assessed using two-dimensional analysis and S.I. moment frames; n_{C1} and n_{C2} are the number of collapsed cases in directions 1 and 2, respectively (shown in Figure 6); and n_{GM} is the total number of selected ground motions (25 for the current study).

In a three-dimensional structure or building, the collapse of a moment frame in one of the lateral directions will result in the collapse of the building. Thus, it is more appropriate to assume the collapses of the two moment frames as fully dependent. The building collapse probability assuming the two moment frames are fully dependent is expressed as follows:

$$P_{P3D}(C|IM) = \frac{n_{C1 \cup C2}}{n_{GM}} \tag{6}$$

where $P_{P3D}(C|IM)$ is the pseudo-three-dimensional collapse probability at a given intensity measure, assuming the collapses of the two moment frames are fully dependent, and $n_{C1 \cup C2}$ is the number of occurrences of collapse in either direction 1 or direction 2. Equation (6) reflects that the collapse events are not independent in directions 1 and 2 for the studied structural system, even though the structure's responses can be assumed to be independent for these two directions. The relationship also implies that the collapse of seismic frames in one direction is equivalent to the collapse of the whole structure for these structural systems. Equation (6) might be used to predict collapse probability for similar structural systems that are independent in two directions, like shear walls or bracing, using two-dimensional analysis.

Repairability plays an essential role in the prediction of seismic losses for modern buildings. Repairability, however, is only considered in predicting losses related to the building (i.e., structural and nonstructural components). FEMA P-58 makes use of an irreparability model which relates irreparability probability to residual drifts. As stated earlier, the nonlinear models used in the current course of study are incorporated with the IMK hysteresis model. The residual drifts predicted using this model are known to be less reliable [42].

The current study utilized the repairability model developed by Safiey and Pang, which defines repairability as a state in which "repair cost" exceeds "reconstruction cost". The great advantage of this model is the ability to account for various exogenous or external factors (e.g., insurance and heritage values) as well as endogenous or internal factors (e.g., structural system). For simplicity, it was assumed that the building was uninsured. The parameters associated with the repairability model were set to $L_m = n.\ 2000\ USD$, $\lambda_D = n.\ 7000 \frac{USD}{day}$, and $RCV_T = n.\ 504000\ USD$, where n represents the number of stories, L_m is miscellaneous indirect losses, λ_D is the daily downtime loss, and RCV_T is indirect replacement cost. Refer to [43] for more details. The direct replacement cost of the building was predicted based on the maximum repair cost obtained from the corresponding consequence functions.

A total of 39 structural and nonstructural vulnerable components were identified for the studied buildings. The fragility and consequence functions of these components were chosen based on FEMA P-58 provisions. The quantity of the vulnerable nonstructural components was determined according to FEMA P-58 recommendations. Appendix B presents the list of structural and nonstructural components. Some of the component fragility functions are sensitive to peak floor acceleration and some to inter-story drift ratios.

Buildings contain at each floor approximately 1302 square m (14,015 square ft) of office space and are assumed to accommodate fifteen office units, or so-called consequence areas, measuring 71 square m (768 square ft), as shown in Figure 6. A total of 113 content objects from 31 groups are included in one consequence area. The normative quantity for each component, i.e., the quantity for each component per unit gross square area, is estimated based on engineering judgment. The replacement cost is estimated based on the Xactimate 2019 database [44], computer software that estimates the cost of property repairs. The contents and their normative quantities are listed in Appendix C. The component fragility functions for content are developed for two independent major failure modes, namely, sliding or overturning, which are sensitive to peak floor acceleration (more information about fragility function derivation can be found in [40,45]). Heavy and electrical content components are herein considered anchored based on engineering judgment [40,45]. Figure 8 presents fragility functions for one anchored (bookcase) and one unanchored component (chair) under both failure modes. Each content component is assumed to have one damage state if unanchored (DS1); DS1 is defined as excessive sliding (when the maximum displacement exceeds a certain displacement threshold) or overturning. If anchored, however, each content component is assumed to have two damage states (DS1, DS2); DS1 is defined as restraint breakage due to sliding or rocking, and DS2 is defined as excessive sliding or overturning. Each content component loss is determined by first calculating the loss due to each failure mode and then considering the maximum of the two modes.

Each component is also represented by a consequence function. Based on engineering judgment, the content consequence function is assumed to be normally distributed with the damage ratio as a median and 20% variance to define the uncertainty of the repair cost. In the case of restraint breakage (DS1 for anchored components), the damage ratio is the restrainer replacement cost ratio for all anchored components. In the case of excessive sliding or overturning (DS2 for anchored components or DS1 for unanchored components), the damage ratio depends on the content type. For example, glassware is expected to have 100% damage if overturned, whereas chairs will incur less damage. The damage ratio is assigned to contents as follows: 30% for furniture, 80% for electrical components, and

100% for glassware [46]. Figure 8 presents the consequence function for the two selected components (chair and bookcase).

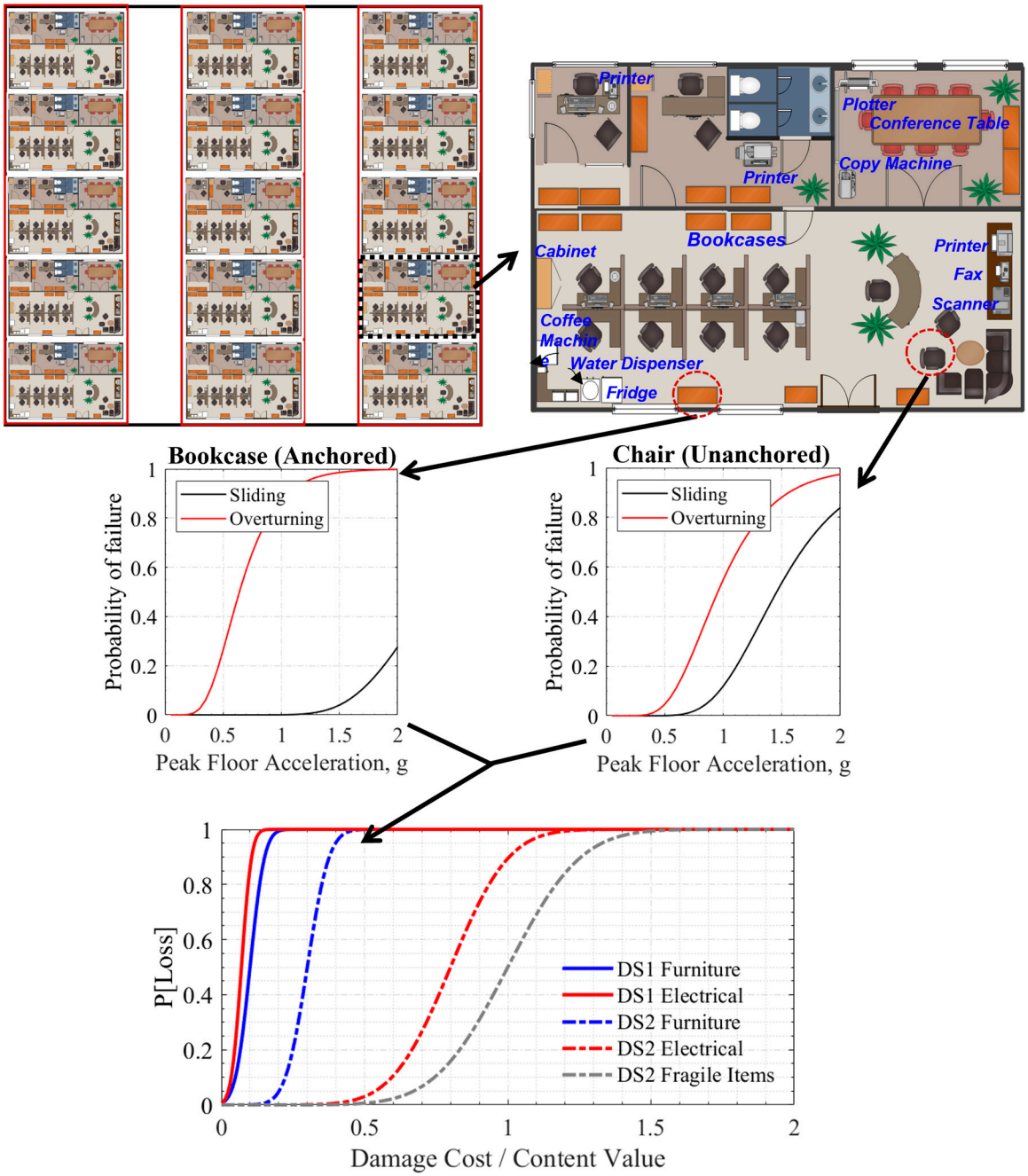

Figure 8. Schematic illustration of content damage and loss assessment.

In the first step, the vulnerability function of each archetype, defined as the mean economic losses versus the spectral acceleration as an intensity measure, is studied. Figure 9 presents the vulnerability of each archetype separately for long- and short-duration shakings. Each plot includes the collapse losses together with content and building vulnerability functions. The building or content loss ratio is the mean total loss divided by the total replacement cost (replacement value). Broadly speaking, the trends of collapse, content, and building losses are similar. The predicted mean values of content and building losses are similar for different heights under long- and short-duration shakings. To be more specific, building losses are higher than content losses for the 2-story building; however,

this trend is the opposite for 4- and 8-story buildings. For taller buildings, higher content losses are observed at lower levels of shaking. Nonetheless, this trend was reversed for this building archetype at spectral accelerations between 0.4 to 0.6 g, except for SMF20 under long-duration ground motions.

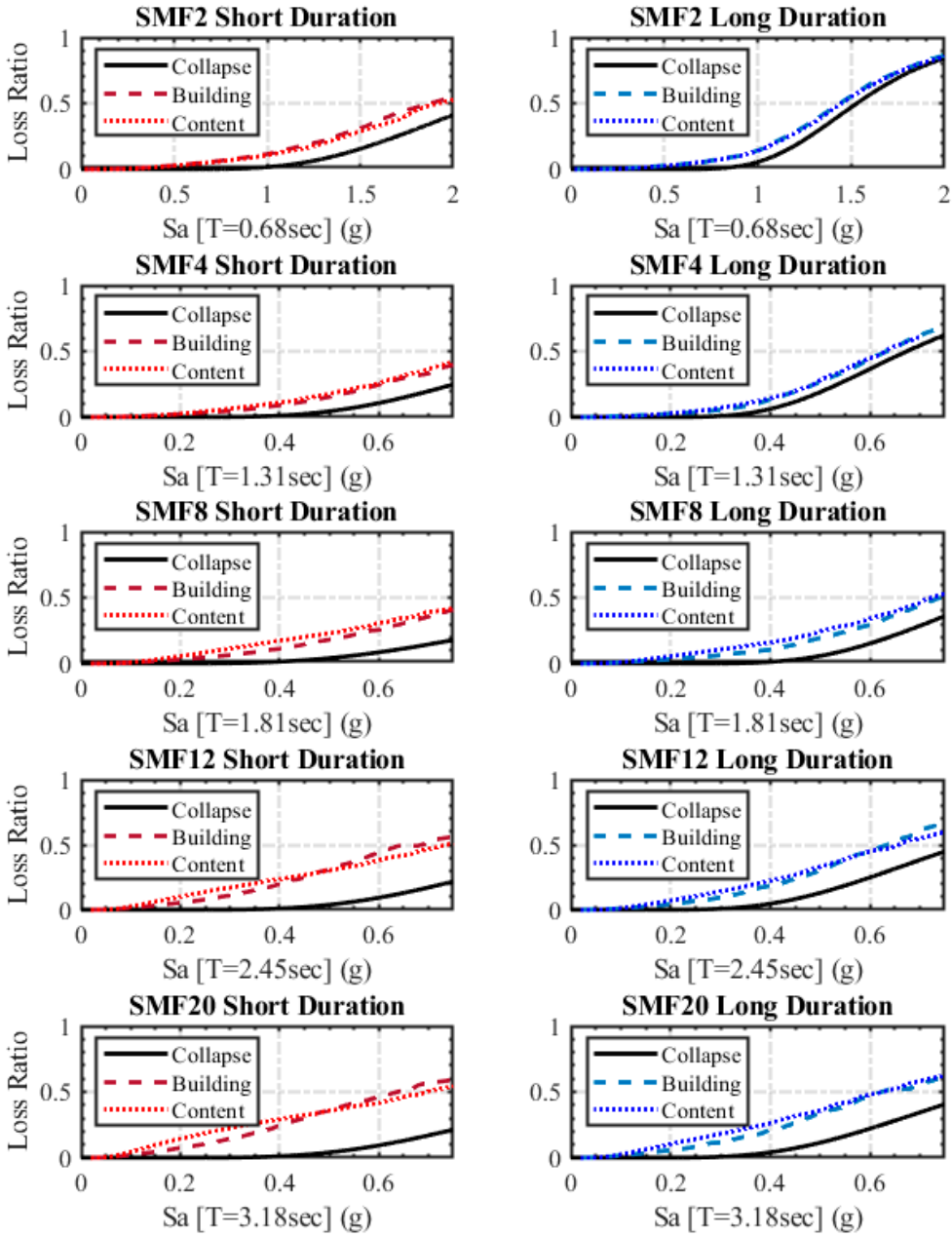

Figure 9. Building and content earthquake vulnerability functions for the studied buildings under short- and long-duration shakings. Each subplot presents loss ratios for each building under a specific set of ground motions.

To facilitate studying the relationship between height and incurred losses at different levels of ground shaking, three ground motion levels (SLE, DBE, and MCE_R) were chosen to represent different severity levels of seismic events. Figure 10 presents the collapse losses for the studied steel frame buildings at these three levels of shaking. Notably, long-duration shaking resulted in higher collapse losses than short-duration shaking. The collapse risk is highest for a 4-story building, as discussed earlier. Figures 10 and 11 also reveal that the trend of content loss from SLE and DBE levels is not downward for heights greater than

4-story. As discussed earlier, the content components are solely sensitive to acceleration. The contribution of collapse to content loss is negligible for these buildings at SLE and DBE. Another observation indicates that short-duration losses at these levels are higher than long-duration losses, because longer shaking durations and longer periods resulted in lower peak floor accelerations (PFAs) compared with short-duration ground motions, which is consistent with the results of an earlier study [47]. This is because of the expeditious release of energy for short-duration shakings (crustal faults), as reported in other studies [47,48].

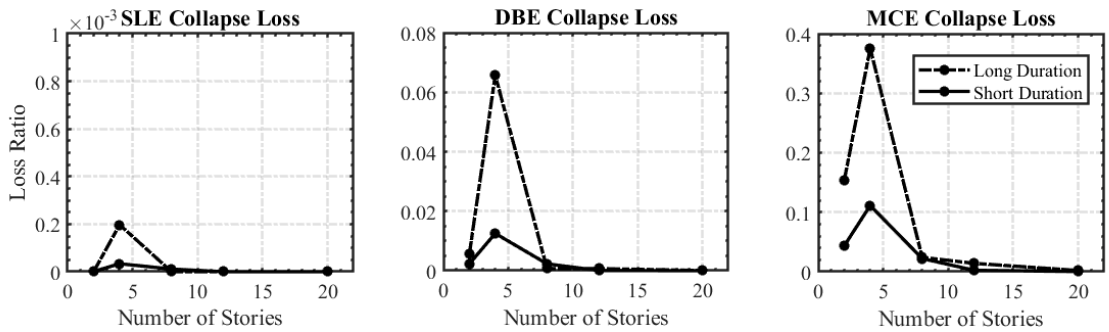

Figure 10. Building and content earthquake collapse losses at different levels of ground shaking. Each subplot presents loss ratios versus building height at different levels of ground motions.

A further step is taken by calculating and comparing each archetype's AAL, which can be computed using the following relationship inferred from FEMA P-58 provisions:

$$AAL = \int \lambda(L)dL = \iint P(L > l|IM)d\lambda(IM)dL \tag{7}$$

where AAL stands for average annual loss, $\lambda(L)$ is the annual frequency of exceedance at a given loss, $P(L > l|IM)$ is the probability of exceeding a certain amount of loss at a specific shaking intensity, and $\lambda(IM)$ is the annual frequency of exceedance of a given shaking intensity, which is known as the hazard curve of the site of the building. To estimate the total average annual loss (AAL_T), we propose breaking it down into two parts, the first being AAL_{LD}, defined as the contributions of long-duration shakings (i.e., subduction faults), and the second one being AAL_{SD}, defined as the contributions of short-duration shakings (i.e., crustal faults). This approach separates the contribution of long- and short-duration earthquakes considered earlier by researchers to determine the annual collapse rate [11]. The described relationship can be mathematically expressed as:

$$AAL_T = AAL_{LD} + AAL_{SD} \tag{8}$$

Contributions of long- and short-duration ground motions to the total AAL can be estimated separately using Equation (7) substituted into Equation (8), as follows:

$$AAL_T = \iint P_{LD}(L > l|IM)d\lambda_{LD}(IM)dL + \iint P_{SD}(L > l|IM)d\lambda_{SD}(IM)dL \tag{9}$$

where $P_{LD}(L > l|IM)$ and $P_{SD}(L > l|IM)$ can be predicted using the building-specific loss assessment for each building under long- and short-duration ground shaking sets, respectively. $\lambda_{LD}(IM)$ and $\lambda_{SD}(IM)$ are hazard curves for the building site for long-duration (i.e., subduction) and short-duration (i.e., crustal) ground motions. The event-type-specific hazard curve of Seattle, WA, with soil type D [49] was used to compute AALs for the studied buildings. Figure 12 shows the seismic hazard curves for the building site disaggregated as the short-duration (crustal) and long-duration (subduction) hazard curves for a building with a period of 1.31 s. Crustal events consist of gridded and fault event types, while subduction events encompass interface and slab event types [50]. Bradley et al.'s parametric hazard model is utilized to facilitate the numerical implementation of the

proposed method [51]. The annual frequency of collapse (λ_C) of the buildings is determined using the same strategy:

$$\lambda_C = \int P_{CLD}(IM) d\lambda_{LD}(IM) dIM + \int P_{CSD}(IM) d\lambda_{SD}(IM) dIM \quad (10)$$

wherein P_{CLD}(IM) and P_{CSD}(IM) are the collapse fragility functions for the building obtained from IDA and expressed in the format of the lognormal cumulative distribution function under long- and short-duration sets of ground motions, respectively. Figure 13 presents the annual frequency of collapse and AAL for each building. Clearly, the trends of content and building AALs under short- and long-duration ground motions are similar to those of corresponding annual frequencies of collapse.

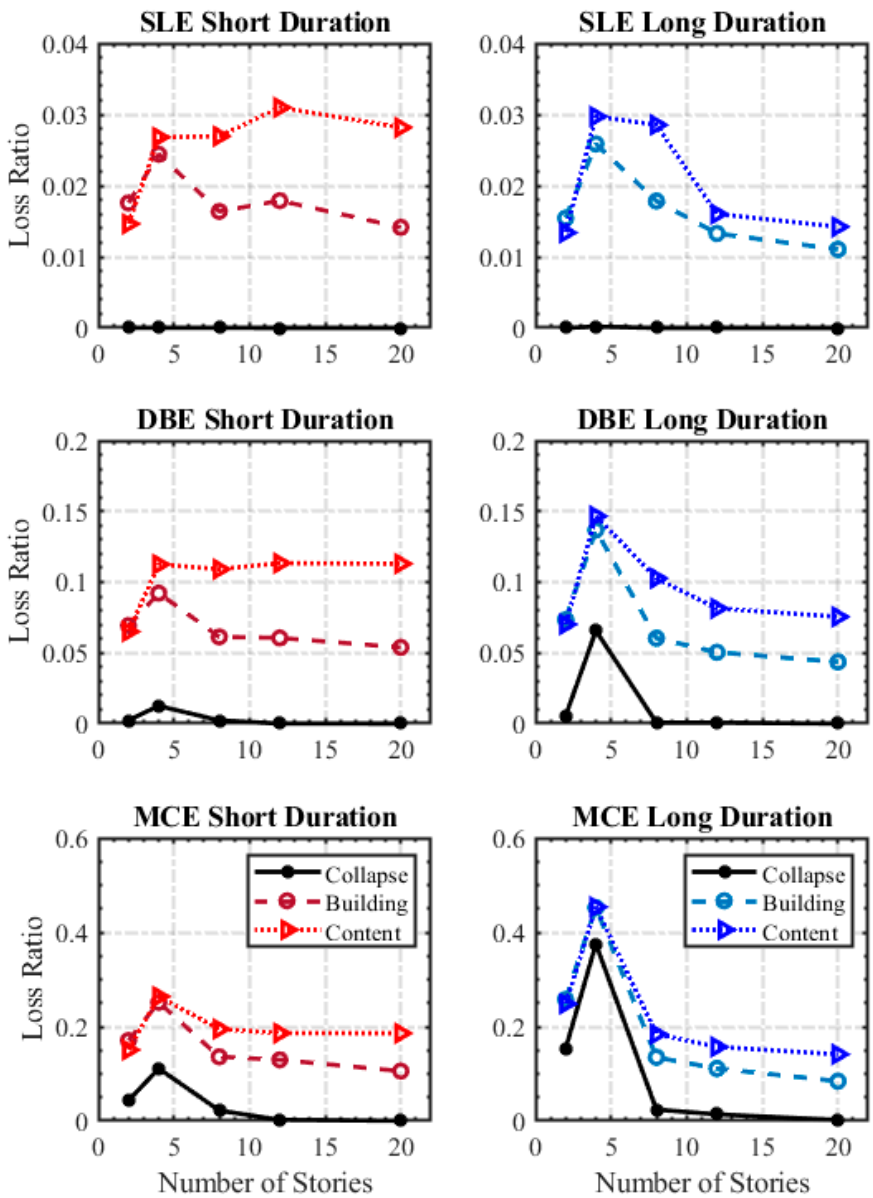

Figure 11. Building and content earthquake losses at different levels of ground shaking. Each subplot presents loss ratios for each set of ground motions at different levels of ground motions for different building heights.

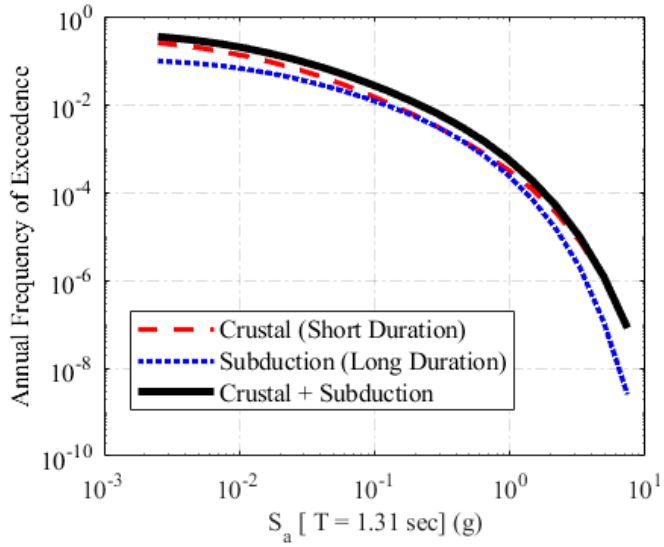

Figure 12. Event-type-specific seismic hazard curves for Seattle, WA, for subduction and crustal zones.

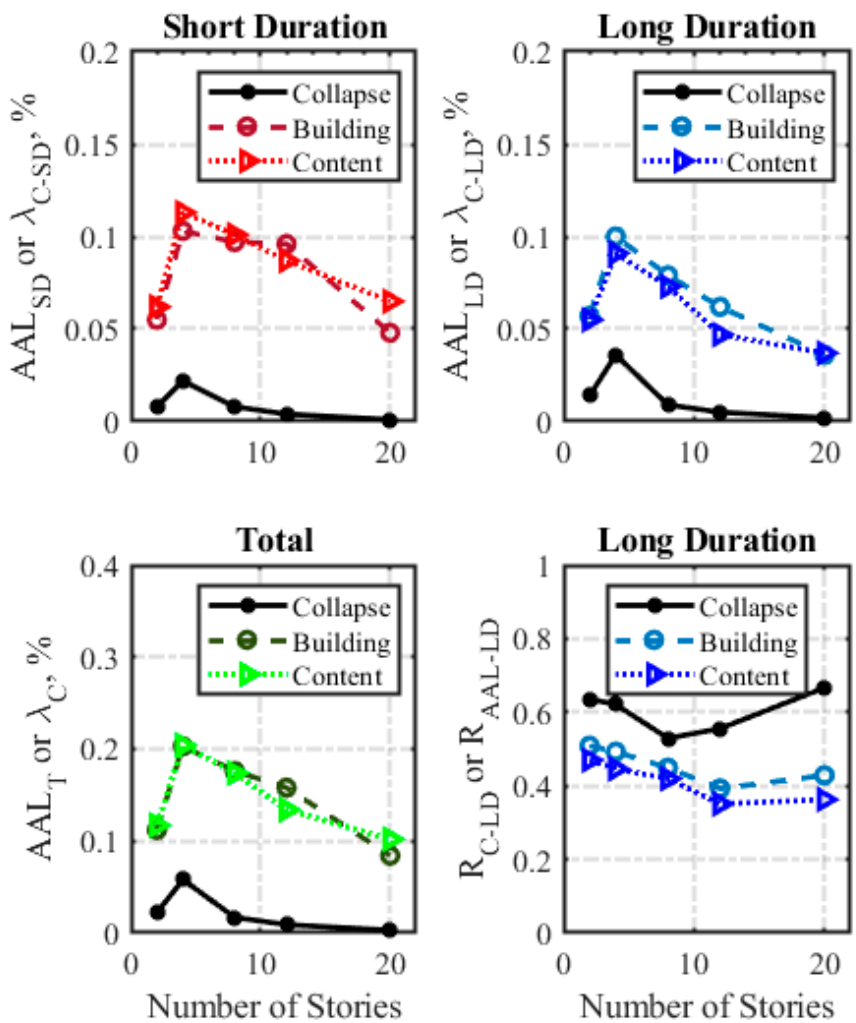

Figure 13. Building and content AAL and annual frequency of collapse. The top subplots present annualized losses under short- and long-duration ground motions versus the building height. The lower subplot on the left side presents total annualized losses for different building heights. The lower right subplot presents the contribution of long-duration ground motions to the incurred losses for different building heights.

The following two ratios are introduced to quantify the contribution of long-duration ground motions on the total *AAL* and annual frequencies of collapse:

$$R_{AAL-LD} = \frac{AAL_{LD}}{AAL_T} \tag{11}$$

$$R_{C-LD} = \frac{\lambda_{C-LD}}{\lambda_C} \tag{12}$$

where R_{AAL-LD} and R_{C-LD} are the contributions of long-duration ground motions on AAL_T and λ_C, respectively. Figure 13 provides the estimates of these two ratios for all studied buildings. As can be seen, the contribution of long-duration earthquakes to the annual frequency of collapse is always more significant than that of short-duration earthquakes, which can be explained through the higher energy dissipation from a larger number of cycles which results in more deterioration and, accordingly, higher collapse rates induced by long-duration ground motions.

The annual frequency of collapse is the primary concern of design codes like ASCE 7–16 [31], which target a uniform collapse risk to preserve the same level of life safety across the country. Figure 13 also reveals that the contribution of long-duration records to the predicted AAL values for either building or content is always smaller than that of short-duration records. The only exception is SMF2, with an estimated R_{AAL-LD} for the building of slightly greater than 0.5. Moreover, the following relationship can be deduced from Figure 13 for the studied buildings:

$$R^{Content}_{AAL-LD} < R^{Building}_{AAL-LD} < R_{C-LD} \tag{13}$$

where $R^{Content}_{AAL-LD}$ and $R^{Building}_{AAL-LD}$ are the contributions of long-duration ground motions to AAL_T predicted for content and building, respectively. The above relationship indicates that long-duration ground motions for the studied buildings contributed less to the *AAL* of content than that of buildings. AALs are controlled mainly by losses at lower motion levels. Content components are sensitive to peak floor acceleration. Therefore, the higher accelerations developed by short-duration ground motions at the lower levels of shaking, also reported by [47], could explain why long-duration ground motions make the lowest contribution to content losses. Figure 13 further reveals relatively higher losses occurring to the content under short-duration ground motions at SLE, which represents low-level shakings.

Average annual losses are of great importance to managers, stakeholders, and insurance carriers. Two separate coverages of an earthquake insurance policy for building properties typically protect building losses ("coverage A" or "damage to house") and content losses ("coverage C" or "personal property"). The results show that for the special steel moment frames studied in this paper, regardless of building height, long-duration ground motions had a greater impact on the insured properties of the building than the content.

5. Conclusions

Most prior research has focused almost exclusively on the impact of long-duration ground motion on building collapse, especially in the Pacific Northwest region. Even though several authors have reported that long-duration shakings amplify collapse risk, its impact on non-collapse risk from building and content damages is still lacking in the literature. To fill this knowledge gap, the current study has provided new results on the collapse and non-collapse risk of steel moment frames. This research examined the influence of ground motion duration on the seismic economic risk of five modern steel moment frame buildings with heights ranging from two to 20 stories.

The previous studies highlight the importance of ground motion duration in assessing the performance of structural systems. An approach for selecting and scaling ground motions was proposed for researchers and practitioners when applying the guidelines of

FEMA P-695 and FEMA P-58 to quantify the seismic performance of a building. The ground motion selection approach is a FEMA P-695 modified approach in which the spectral shape of the bi-directional components of short-duration ground motions is matched with that of long-duration ones. A component-based loss estimation methodology is adopted to predict seismic losses sustained by buildings impacted by short- and long-duration ground motions. Key results and conclusions can be summarized as follows:

- A simple yet effective approach was proposed to provide a hazard-consistent estimate of AAL for building properties. The approach was used to predict this parameter for studied buildings providing insights into the contribution of long-duration ground motions to the aggregate economic losses;
- The proposed scaling methodology for long-duration ground motions is applied to the FEMA P-695 approach in a way compatible with FEMA P-58 component-based loss modeling. It proves practical for comparisons with the risk associated with short-duration ground motions;
- Long-duration ground motion reduces the collapse capacity for all the studied steel moment frames, where the collapse capacity was 31%, 29%, 31%, 26%, and 23% lower than that of the 2-, 4-, 8-, 12-, and 20-story steel moment frames under short-duration ground motions, respectively. This result aligns with the conclusions of other similar works [7,16–18];
- From moderate to extreme ground motion intensities, long duration exerts a higher impact on the building's total dollar loss. The main reason for this increase is the higher contribution of collapse loss, as long-duration shakings result in higher energy dissipation and deterioration. The influence is more apparent in low- and mid-rise models;
- Contents have higher loss ratios at lower shaking levels than structural and nonstructural components; however, the loss ratios for both building and content are close in value;
- Long-duration ground motion does not play a significant role in the peak floor acceleration of buildings of different heights. Hence, it does not influence content losses, which depend solely on peak floor acceleration;
- The average annual collapse loss is higher for long-duration ground motions than for short-duration shakings. The long-duration ground motions for the studied buildings made a lower contribution to the AALs of content than those of the building.

The scope of this study was only limited to modern steel structures. Therefore, further studies are needed to investigate the influence of long-duration ground motions on economic risk for different structural systems designed for different ductility levels. Furthermore, the study focuses on moment frame buildings with symmetrical floor plans devoid of specific characteristics such as plan irregularities or soft stories. Exploring the impact of such features on a building could be a potential area for future investigation.

Author Contributions: Conceptualization, A.S., S.M. and W.P.; methodology, A.S., S.M. and W.P.; software, A.S. and S.M.; validation, A.S., S.M. and W.P.; formal analysis, A.S. and S.M.; investigation, A.S. and S.M.; resources, W.P.; data curation, A.S. and S.M.; writing—original draft preparation, A.S., S.M. and W.P.; writing—review and editing, A.S., S.M. and W.P.; visualization, A.S. and S.M.; supervision, W.P.; project administration, W.P.; funding acquisition, W.P. All authors have read and agreed to the published version of the manuscript.

Funding: This research received no external funding.

Data Availability Statement: Data may be accessible upon request from the authors.

Acknowledgments: We acknowledge Clemson University for the generous allotment of computing time on the Palmetto Cluster. Any opinions, findings, conclusions, or recommendations expressed herein are only of the authors.

Conflicts of Interest: Author Sereen Majdalaweyh was employed by the company Karen Clark and Company. The remaining authors declare that the research was conducted in the absence of any commercial or financial relationships that could be construed as a potential conflict of interest.

Appendix A

Appendix A provides the list of selected long- and short-duration ground motions.

Table A1. List of selected ground motions.

#	Long-Duration Records			Short-Duration Records		
	Event	**Station**	**MF**	**Event**	**Station**	**NM**
1	1992 Landers	Coachella Canal	0.71	1999 Chi-Chi, Taiwan-06	CHY100	1.19
2	1992 Landers	Indio—Jackson Road	0.41	1992 Cape Mendocino	Petrolia	0.17
3	2011 Tohoku, Japan	Yanagawa	0.41	2004 Niigata, Japan	NIGH10	1.44
4	2011 Tohoku, Japan	Iitate	0.44	1987 Whittier Narrows-01	Orange Co. Reservoir	1.36
5	2003 Hokkaido, Japan	Hayakita	0.51	2010 El Mayor–Cucapah	San Diego—45th and Orange	2.46
6	2010 Maule, Chile	Santiago La Florida	0.84	1986 Chalfant Valley-01	Bishop—LADWP South St	1.39
7	1999 Chi-Chi, Taiwan	CHY052	0.94	1986 Taiwan SMART1(45)	SMART1 O02	0.48
8	1979 Imperial Valley-06	Victoria	1.41	2003 Chi-Chi, Taiwan-06	TCU129	0.83
9	1999 Kocaeli, Turkey	Bursa Tofas	0.51	1986 Taiwan SMART1(45)	SMART1 I12	0.37
10	1999 Kocaeli, Turkey	Atakoy	0.80	1999 Chi-Chi, Taiwan-04	CHY046	0.93
11	2011 Tohoku, Japan	ASHIRO	1.01	1992 Big Bear-01	San Bernardino	1.18
12	2003 Hokkaido, Japan	Hobetsu	0.54	1987 Superstition Hills-02	Poe Road	0.32
13	2011 Tohoku, Japan	Kawagoe	0.59	1979 Imperial Valley-06	El Centro Array #1	0.84
14	2011 Tohoku, Japan	Nihommatsu	0.34	1987 Whittier Narrows-01	Canyon Country—W Lost Canyon	1.51
15	2003 Hokkaido, Japan	Shihoro	0.43	1979 Imperial Valley-06	Holtville Post Office	0.21
16	2003 Hokkaido, Japan	Oiwake	0.39	1999 Hector Mine	Mill Creek Ranger Station	0.91
17	2010 El Mayor-Cucapah	Chihuahua	0.33	2010 Darfield, New Zealand	DORC	1.00
18	2011 Tohoku, Japan	Kawamata	0.59	1987 Whittier Narrows-01	El Monte—Fairview Av	1.04
19	2011 Tohoku, Japan	Ichinoseki	0.27	1994 Northridge	LA—Fletcher Dr	1.21
20	2011 Tohoku, Japan	Sakunami	0.88	1999 Chi-Chi, Taiwan-02	TCU067	0.84
21	1999 Chi-Chi, Taiwan	CHY004	1.13	1994 Northridge-01	LA—Pico and Sentous	1.16
22	1992 Landers	Mission Creek Fault	1.15	1994 Northridge-01	Inglewood—Union Oil	1.30
23	2000 Chi-Chi, Taiwan	CHY107	0.55	Victoria, Mexico	Chihuahua	0.51
24	1992 Landers	Downey—Maint Bldg	1.10	2004 Parkfield-02	Coaling—Priest Valley	2.62
25	2002 Denali, Alasaka	Geophysic. Obs CIGO	1.48	2007 Chuetsu-oki, Japan	Yanagishima paddocks	0.48

Appendix B

This appendix provides the list of vulnerable structural and nonstructural components for the studied buildings. Units are as per FEMA P-58 provisions.

Table A2. List of vulnerable structural and nonstructural components.

#	Component	Description	Floor	Quantity
1	B1031.001	Bolted shear tab gravity connections	All except first	80
2	B1031.011	Steel column base plates	Second	16
3	B1035	Post-Northridge RBS connection	All except first	16
5	B1049.031	Post-tensioned concrete flat slabs	All except first	16
6	B1031.021a	Column splices	Based on drawings	16
7	B2022.001	Curtain walls	All except first	280
8	B3011.011	Concrete tile roof	Roof	37.8
9	C2011.031a	Hybrid stair	All except first	2
10	C3011.001a	Wall partition, type: gypsum + wallpaper	All except first	3.1
11	C3011.002a	Wall partition, type: gypsum + ceramic tile	All except first	0.2
12	C3032.003d	Suspended Ceiling	All except first	5.04
13	D1014.011	Traction elevator	First	1
14	D2021.014a	Cold or hot potable piping fragility	All except first	1.76
15	D2021.014b	Cold or hot potable bracing fragility	All except first	1.76
16	D2021.024a	Cold or hot potable water piping, piping fragility	All except first	0.63
17	D2021.024b	Cold or hot potable water piping bracing fragility	All except first	0.63
18	D2022.014a	Heating hot water piping, piping fragility	All except first	0.07
19	D2022.014b	Heating hot water piping bracing fragility	All except first	0.07
20	D2022.024a	Heating hot water piping, piping fragility	All except first	0.07
21	D2022.024b	Heating hot water piping bracing fragility	All except first	0.07
22	D2031.024a	Sanitary waste piping, piping fragility	All except first	0.8
23	D2031.024b	Sanitary waste piping bracing fragility	All except first	0.8
24	D3031.013j	Chiller anchorage fragility	All except first	0.05
25	D3031.013k	Chiller capacity equipment fragility	All except first	0.05
26	D3031.022j	Cooling tower anchorage fragility	All except first	0.05
27	D3031.022k	Cooling tower equipment fragility	All except first	0.05
28	D3041.011d	HVAC galvanized sheet metal ducting	All except first	1.05
29	D3041.012d	HVAC galvanized sheet metal ducting—6 sq. ft cross sectional area or greater	All except first	0.28
30	D3041.032c	HVAC drops	All except first	13
31	D3041.041b	Variable air volume	All except first	7
32	D3052.013d	Air handling unit anchorage fragility	All except first	1.2
33	D3052.013e	Air handling unit equipment fragility	All except first	1.2
34	D4011.024a	Fire sprinkler water piping, piping fragility	All except first	2.8
35	D4011.034a	Fire sprinkler drop standard	All except first	2
36	D5012.023d	Low voltage switchgear anchorage fragility	All except first	0.005
37	D5012.023e	Low voltage switchgear equipment fragility	All except first	0.005
38	B1031.001	Bolted shear tab gravity connections	All except first	80
39	B1031.011	Steel column base plates	Second	16
40	B1035	Post-Northridge RBS connection	All except first	16

Appendix C

This appendix provides the list of vulnerable content components for the studied buildings.

Table A3. List of contents and restrainers characteristics

#	Component	Cost, USD/m^2
1	Beverage dispenser	0.27
2	Coffee machine	0.71
3	Under counter refrigerator	1.58
5	Desktop computer	5.33
6	Plotter	8.67
7	Laptop	5.33
8	Monitor	4.00
9	Photo Printer	1.07
10	LCD 20–24 in	2.00
11	Camcorder digital camera	4.07
12	Countertop microwave	0.93
13	Printer and Fax machine	0.80
14	Stand-alone projection screen	4.00
15	Projector	13.33
16	Scanner	1.13
17	Conference telephone	2.67
18	Laser Jet printer	1.93
19	Commercial grade printer	26.67
20	Office jet printer	0.67
21	DVD Drive	0.27
22	Big Glass	0.04
23	File cabinets	1.53
24	Bookcases	0.87
25	Vase	0.24
26	Coffee pot	0.19
27	Chair	1.13
28	Client Seating	1.20
29	Desk	0.93
30	Mug	0.09
31	Conference table	2.93

References

1. Chandramohan, R.; Baker, J.W.; Deierlein, G.G. Accounting for the Influence of Ground Motion Response Spectral Shape and Duration in the Equivalent Lateral Force Design Procedure. In Proceedings of the US National Conference on Earthquake Engineering, Los Angeles, CA, USA, 25–29 June 2018; Volume 7, pp. 4006–4016.
2. FEMA. *HAZUS-MH MR4 Technical Manual*; FEMA: Washington, DC, USA, 2003.
3. van de Lindt, J.W.; Goh, G. Effect of Earthquake Duration on Structural Reliability. *Eng. Struct.* **2004**, *26*, 1585–1597. [CrossRef]
4. Hou, H.; Qu, B. Duration Effect of Spectrally Matched Ground Motions on Seismic Demands of Elastic Perfectly Plastic SDOFS. *Eng. Struct.* **2015**, *90*, 48–60. [CrossRef]

5. Molazadeh, M.; Saffari, H. The Effects of Ground Motion Duration and Pinching-Degrading Behavior on Seismic Response of SDOF Systems. *Soil Dyn. Earthq. Eng.* **2018**, *114*, 333–347. [CrossRef]
6. Bravo-Haro, M.A.; Liapopoulou, M.; Elghazouli, A.Y. Seismic Collapse Capacity Assessment of SDOF Systems Incorporating Duration and Instability Effects. *Bull. Earthq. Eng.* **2020**, *18*, 3025–3056. [CrossRef]
7. Liapopoulou, M.; Bravo-Haro, M.A.; Elghazouli, A.Y. The Role of Ground Motion Duration and Pulse Effects in the Collapse of Ductile Systems. *Earthq. Eng. Struct. Dyn.* **2020**, *49*, 1051–1071. [CrossRef]
8. Hassan, A.L.; Billah, A.M. Influence of Ground Motion Duration and Isolation Bearings on the Seismic Response of Base-Isolated Bridges. *Eng. Struct.* **2020**, *222*, 111129. [CrossRef]
9. Raghunandan, M.; Liel, A.B. Effect of Ground Motion Duration on Earthquake-Induced Structural Collapse. *Struct. Saf.* **2013**, *41*, 119–133. [CrossRef]
10. Fairhurst, M.; Bebamzadeh, A.; Ventura, C.E. Effect of Ground Motion Duration on Reinforced Concrete Shear Wall Buildings. *Earthq. Spectra* **2019**, *55*, 311–331. [CrossRef]
11. Raghunandan, M.; Liel, A.B.; Luco, N. Collapse Risk of Buildings in the Pacific Northwest Region Due to Subduction Earthquakes. *Earthq. Spectra* **2015**, *31*, 2087–2115. [CrossRef]
12. Pan, Y.; Ventura, C.E.; Liam Finn, W.D. Effects of Ground Motion Duration on the Seismic Performance and Collapse Rate of Light-Frame Wood Houses. *J. Struct. Eng.* **2018**, *144*, 04018112. [CrossRef]
13. Pan, Y.; Ventura, C.E.; Finn, W.D.L.; Xiong, H. Effects of Ground Motion Duration on the Seismic Damage to and Collapse Capacity of a Mid-Rise Woodframe Building. *Eng. Struct.* **2019**, *197*, 109451. [CrossRef]
14. Pan, Y.; Ventura, C.E.; Tannert, T. Damage Index Fragility Assessment of Low-Rise Light-Frame Wood Buildings under Long Duration Subduction Earthquakes. *Struct. Saf.* **2020**, *84*, 101940. [CrossRef]
15. Jafari, M.; Pan, Y.; Shahnewaz, M.; Tannert, T. Effects of Ground Motion Duration on the Seismic Performance of a Two-Storey Balloon-Type CLT Building. *Buildings* **2022**, *12*, 1022. [CrossRef]
16. Chandramohan, R.; Baker, J.W.; Deierlein, G.G. Quantifying the Influence of Ground Motion Duration on Structural Collapse Capacity Using Spectrally Equivalent Records. *Earthq. Spectra* **2016**, *32*, 927–950. [CrossRef]
17. Hwang, S.H.; Mangalathu, S.; Jeon, J.S. Quantifying the Effects of Long-Duration Earthquake Ground Motions on the Financial Losses of Steel Moment Resisting Frame Buildings of Varying Design Risk Category. *Earthq. Eng. Struct. Dyn.* **2021**, *50*, 1451–1468. [CrossRef]
18. Zengin, E.; Abrahamson, N.A.; Kunnath, S. Isolating the Effect of Ground-Motion Duration on Structural Damage and Collapse of Steel Frame Buildings. *Earthq. Spectra* **2020**, *36*, 718–740. [CrossRef]
19. Pang, W.; Safiey, A.; Majdalaweyh, S.; Ziaei, E.; Rokneddin, K.; Javanbarg, M. Ground Motion Duration Effects on the Seismic Risk Assessment of Wood Light-Frame Buildings. In Proceedings of the 17th World Conference on Earthquake Engineering, Sendai, Japan, 27 September–2 October 2020.
20. Belejo, A.; Barbosa, A.R.; Bento, R. Influence of Ground Motion Duration on Damage Index-Based Fragility Assessment of a Plan-Asymmetric Non-Ductile Reinforced Concrete Building. *Eng. Struct.* **2017**, *151*, 682–703. [CrossRef]
21. Shahi, S.K.; Baker, J.W. NGA-West2 Models for Ground Motion Directionality. *Earthq. Spectra* **2014**, *30*, 1285–1300. [CrossRef]
22. Otárola, K.; Sousa, L.; Gentile, R.; Galasso, C. Impact of Ground-Motion Duration on Nonlinear Structural Performance: Part II: Site- and Building-Specific Analysis. *Earthq. Spectra* **2023**, *39*, 860–888. [CrossRef]
23. Otárola, K.; Gentile, R.; Sousa, L.; Galasso, C. Impact of Ground-Motion Duration on Nonlinear Structural Performance: Part I: Spectrally Equivalent Records and Inelastic Single-Degree-of-Freedom Systems. *Earthq. Spectra* **2023**, *39*, 829–859. [CrossRef]
24. Doughton, S. What If the Megaquake Happens When You're in a Seattle High-Rise? New Study Predicts Stronger Shaking | The Seattle Times. *Seattle Times*, 21 December 2018.
25. *FEMA P-695*; Quantification of Building Seismic Performance Factors. FEMA: Washington, DC, USA, 2009.
26. *FEMA P-58*; Seismic Performance Assessment of Buildings—Methodology. FEMA: Washington, DC, USA, 2012; Volume 1.
27. Ancheta, T.D.; Darragh, R.B.; Stewart, J.P.; Seyhan, E.; Silva, W.J.; Chiou, B.S.-J.; Wooddell, K.E.; Graves, R.W.; Kottke, A.R.; Boore, D.M.; et al. NGA-West2 Database. *Earthq. Spectra* **2014**, *30*, 989–1005. [CrossRef]
28. Aoi, S.; Kunugi, T.; Nakamura, H.; Fujiwara, H. Deployment of New Strong Motion Seismographs of K-NET and KiK-Net. In *Earthquake Data in Engineering Seismology: Predictive Models, Data Management and Networks*; Springer: Berlin/Heidelberg, Germany, 2011; pp. 167–186.
29. Archuleta, R.J.; Steidl, J.; Squibb, M. The COSMOS Virtual Data Center: A Web Portal for Strong Motion Data Dissemination. *Seismol. Res. Lett.* **2006**, *77*, 651–658. [CrossRef]
30. Molina Hutt, C.; Marafi, N.; Berman, J.; Eberhard, M. Effects of Basins during Subduction Earthquakes on the Collapse Fragility of Existing Tall Steel Buildings. In Proceedings of the 11th National Conference on Earthquake Engineering 2018, NCEE 2018: Integrating Science, Engineering, and Policy, Los Angeles, CA, USA, 25–29 June 2018; Volume 10, pp. 5982–5992.
31. *ASCE Minimum Design Loads and Associated Criteria for Buildings and Other Structures*; ASCE: Reston, VA, USA, 2016.
32. Mazzoni, S.; McKenna, F.; Scott, M.H.; Fenves, G.L. *OpenSees Command Language Manual*; Pacific Earthquake Engineering Research Center (PEER): Berkeley, CA, USA, 2009. Available online: https://opensees.berkeley.edu/OpenSees/manuals/usermanual/index.html (accessed on 1 May 2024).

33. *ANSI/AISC Prequalified Connections for Special and Intermediate Steel Moment Frames for Seismic Applications with Supplement No. 1*; ANSI/AISC: Chicago, IL, USA, 2018. Available online: https://www.aisc.org/globalassets/aisc/publications/standards/a358-18w.pdf (accessed on 1 May 2024).
34. *PEER/ATC PEER/ATC 72-1—Modeling and Acceptance Criteria for Seismic Design and Analysis of Tall Buildings*; ATC: Redwood City, CA, USA, 2010. Available online: https://peer.berkeley.edu/sites/default/files/peer-atc-72-1_report.pdf (accessed on 1 May 2024).
35. Elkady, A. *Collapse Risk Assessment of Steel Moment Resisting Frames Designed with Deep Wide-Flange Columns in Seismic Regions*; McGill University: Montreal, QC, Canada, 2016.
36. Elkady, A.; Lignos, D.G. Modeling of the composite action in fully restrained beam-to-column connections: Implications in the seismic design and collapse capacity of steel special moment frames. *Earthq. Eng. Struct. Dyn.* **2014**, *43*, 1935–1954. [CrossRef]
37. Elkady, A.; Lignos, D.G. Effect of gravity framing on the overstrength and collapse capacity of steel frame buildings with perimeter special moment frames. *Earthq. Eng. Struct. Dyn.* **2015**, *44*, 1289–1307. [CrossRef]
38. The MathWorks Inc. MATLAB R2017a. 2017. Available online: https://www.mathworks.com/products/matlab.html (accessed on 1 May 2024).
39. Safiey, A. *Performance-Based Seismic Loss Estimation of Buildings*; Clemson University: Clemson, SC, USA, 2020.
40. Majdalaweyh, S.; Pang, W. Empirical Seismic Fragility Assessment and Optimal Risk Mitigation of Building Contents. *Eng. Struct.* **2022**, *259*, 114183. [CrossRef]
41. Pang, W.; Majdalaweyh, S.; Safiey, A.; Rokneddin, K.; Prabhu, S.; Javanbarg, M.; Ziaei, E. A Probabilistic Casualty Model to Include Injury Severity Levels in Seismic Risk Assessment. In Proceedings of the 17th World Conference on Earthquake Engineering, Sendai, Japan, 27 September–2 October 2020.
42. Cook, D.T. *Advancing Performance-Based Earthquake Engineering for Modern Resilience Objectives*; University of Colorado Boulder: Boulder, CO, USA, 2021.
43. Safiey, A.; Pang, W. A New Approach to Assessing Reparability for Seismic Risk Assessment of Buildings. *Earthq. Spectra* **2021**, *37*, 284–303. [CrossRef]
44. Xactware Software for Estimating All Phases of Building and Repair. Available online: https://www.xactware.com/ (accessed on 22 August 2021).
45. Majdalaweyh, S.; Pang, W.; Safiey, A.; Ziaei, E.; Rokneddin, K.; Javanbarg, M.; Prabhu, S. Seismic Vulnerability Assessment of Anchored Block Type Contents Due to Sliding and Overturning. In Proceedings of the 12th Canadian Conference on Earthquake Engineering, Quebec City, QC, Canada, 17–20 June 2019; pp. 1–8.
46. Jaimes, M.A.; Reinoso, E.; Esteva, L. Seismic Vulnerability of Building Contents for a Given Occupancy Due to Multiple Failure Modes. *J. Earthq. Eng.* **2013**, *17*, 658–672. [CrossRef]
47. Kiani, J.; Pezeshk, S. Sensitivity Analysis of the Seismic Demands of RC Moment Resisting Frames to Different Aspects of Ground Motions. *Earthq. Eng. Struct. Dyn.* **2017**, *46*, 2739–2755. [CrossRef]
48. Hancock, J.; Bommer, J.J. A State-of-Knowledge Review of the Influence of Strong-Motion Duration on Structural Damage. *Earthq. Spectra* **2006**, *22*, 827–845. [CrossRef]
49. Frankel, A.D.; Mueller, C.S.; Barnhard, T.P.; Leyendecker, E.V.; Wesson, R.L.; Harmsen, S.C.; Klein, F.W.; Perkins, D.M.; Dickman, N.C.; Hanson, S.L.; et al. USGS National Seismic Hazard Maps. *Earthq. Spectra* **2000**, *16*, 1–9. [CrossRef]
50. Petersen, M.D.; Shumway, A.M.; Powers, P.M.; Mueller, C.S.; Moschetti, M.P.; Frankel, A.D.; Rezaeian, S.; McNamara, D.E.; Luco, N.; Boyd, O.S.; et al. The 2018 Update of the US National Seismic Hazard Model: Overview of Model and Implications. *Earthq. Spectra* **2020**, *36*, 5–41. [CrossRef]
51. Bradley, B.A.; Dhakal, R.P.; Cubrinovski, M.; Mander, J.B.; MacRae, G.A. Improved Seismic Hazard Model with Application to Probabilistic Seismic Demand Analysis. *Earthq. Eng. Struct. Dyn.* **2007**, *36*, 2211–2225. [CrossRef]